Journal of Hydrology 573 (2019) 49–59

Contents lists available at ScienceDirect

Journal of Hydrology

journal homepage: www.elsevier.com/locate/jhydrol

Research papers

Impacts of future climate change on water resource availability of eastern Australia: A case study of the Manning River basin

Hong Zhang[a,b], Bin Wang[b], De Li Liu[b,c,*], Mingxi Zhang[a,b,d], Puyu Feng[a,b], Lei Cheng[e,f], Qiang Yu[d,a,g,*], Derek Eamus[a]

[a] School of Life Sciences, Faculty of Science, University of Technology Sydney, PO Box 123, Broadway, Sydney, NSW 2007, Australia
[b] NSW Department of Primary Industries, Wagga Wagga Agricultural Institute, Wagga Wagga, NSW 2650, Australia
[c] Climate Change Research Centre and ARC Centre of Excellence for Climate Extremes, University of New South Wales, Sydney, NSW 2052, Australia
[d] State Key Laboratory of Soil Erosion and Dryland Farming on the Loess Plateau, Northwest A&F University, Yangling, Shaanxi 712100, China
[e] State Key Laboratory of Water Resources and Hydropower Engineering Science, Wuhan University, Wuhan 430072, China
[f] Hubei Provincial Collaborative Innovation Center for Water Resources Security, Wuhan 430072, China
[g] College of Resources and Environment, University of Chinese Academy of Science, Beijing 100049, China

ARTICLE INFO

This manuscript was handled by Marco Borga, Editor-in-Chief, with the assistance of Maria-Helena Ramos, Associate Editor

Keywords:
GCMs
Xinanjiang (XAJ) model
Climate change
Eastern Australia
Runoff

ABSTRACT

Hydrological responses of catchments to climate change require detailed examination to ensure sustainable management of both water resources and natural ecosystems. This study evaluated the impacts of climate change on water resource availability of a catchment in eastern Australia (i.e. the Manning River catchment) and analyzed climate-hydrology relationships. For this evaluation, the Xinanjiang (XAJ) model was used and validated to simulate monthly rainfall-runoff relationships of the catchment. Statistically downscaled climate data based on 28 global climate models (GCMs) under RCP8.5 scenarios were used to assess the impacts of climate changes on the Manning River catchment. Our results showed that the XAJ model was able to reproduce observed monthly rainfall-runoff relationships with an $R^2 \geq 0.94$ and a Nash-Sutcliffe Efficiency ≥ 0.92. The median estimates from the ensemble of downscaled GCM projections showed a slight decrease in annual rainfall and runoff for the period 2021–2060 and an increase for the period 2061–2100. Annual actual evapotranspiration was projected to increase slightly, while annual soil moisture content was predicted to decrease in the future. Our results also demonstrated that future changes in seasonal and annual runoff, actual evapotranspiration and soil moisture are largely dominated by changes in rainfall, with a smaller influence arising from changes in temperature. An increase in the values of high runoffs and a decrease in the values of low runoffs predicted from the ensemble of the 28 GCMs suggest increased variability of water resources at monthly and seasonal timescales in the future. A trend of decreasing values in winter runoff and soil moisture content in the future is likely to aggravate possible future reductions in water availability in eastern Australia. These results contribute to the development of adaptive strategies and future policy options for the sustainable management of water resources in eastern Australia.

1. Introduction

Global increases in atmospheric temperature is intensifying hydrological processes (Huntington, 2006; Oki and Kanae, 2006). For example, climate change is associated with changes in rainfall (amount, timing and distribution), increase in rates of evapotranspiration and changes in other climatic variables, and these changes will be amplified in runoff (Chiew et al., 2009; Reshmidevi et al., 2018). As a result, hydrological responses to global climate change have been widely studied in recent years. Thus, Menzel and Bürger (2002) predicted a trend of decreasing mean runoff for a catchment in Germany, while Su et al. (2017) reported that annual average runoff would increase in the 21st century in the upper Yangtze River basin in China. By the end of this century, annual runoff is projected to decrease in parts of southern Africa, the Middle East and southern Europe, while increased annual runoff is projected to occur in high northern latitudes, consistent with large increases in spring and winter rainfall under the RCP8.5 scenario (IPCC, 2013).

* Corresponding authors at: State Key Laboratory of Soil Erosion and Dryland Farming on the Loess Plateau, Northwest A&F University, Yangling, Shaanxi 712100, China (Q. Yu); NSW Department of Primary Industries, Wagga Wagga Agricultural Institute, Wagga Wagga, NSW 2650, Australia (D.L. Liu).
E-mail addresses: de.li.liu@dpi.nsw.gov.au (D.L. Liu), yuq@nwafu.edu.cn (Q. Yu).

https://doi.org/10.1016/j.jhydrol.2019.03.067
Received 19 October 2018; Received in revised form 14 March 2019; Accepted 18 March 2019
Available online 18 March 2019
0022-1694/

Australia has the world's most variable climate (Manolas, 2010; Stokes et al., 2010) and climate change has significantly affected Australian regional water availability and ecosystem health (CSIRO, 2016). Eastern Australia, including the majority (*ca* 80%) of the Australian population, is influenced by large-scale drivers of atmospheric circulation, including the El Niño Southern Oscillation, the Indian Ocean dipole and the southern annular mode (Cleverly et al., 2016), leading to high variability and the frequent occurrence of extensive droughts and floods. For instance, eastern Australia has been subject to considerable climate variability, including the Millennium Drought and the two wettest years on record for Australia (2010–2011), the latter as a result of two strong La Niña events. While several studies have assessed the impacts of climate change on the hydrology of eastern Australia (Chiew et al., 2009; Vaze and Teng, 2011) there have been few detailed studies of impacts of climate change on individual catchments in eastern Australia. Consequently, we examined a catchment representative of eastern Australia to provide detailed insight for future options for water management.

In most studies of the impacts of climate change, Global Climate Models (GCMs) have been the primary means used for global and regional climate simulations (Reshmidevi et al., 2018), especially with the large improvements in climate modelling in recent decades (IPCC, 2014). However, climatic variables simulated from GCMs are often too spatially coarse to be used directly in hydrological models (Jiang et al., 2007). Furthermore, archived daily sequences simulated by GCMs are currently available only for specific periods (time slices) of a few decades (Liu and Zuo, 2012) and for a few GCMs. Therefore, downscaling approaches have to be adopted to transform large-scale GCMs outputs to daily time series at local and regional scales (Liu and Zuo, 2012; Silberstein et al., 2012). Over the last few decades, a series of downscaling methods have been used for this purpose (Ahmed et al., 2013; Diaz-Nieto and Wilby, 2005; Fowler et al., 2007; Frei et al., 2003; Gordon and O'Farrell, 1997; Hewitson and Crane, 2006). Dynamical downscaling and statistical downscaling are the two basic downscaling methods in the one-way coupling of GCMs and hydrological models (Chen et al., 2012; Fowler et al., 2007). Dynamical downscaling models, involving the use of regional numerical models that include full sets of physics (Tang et al., 2016), are highly computationally demanding and restricted to 'time slices', although they have explicit physical meanings (Fowler et al., 2007). In contrast, statistical downscaling models are relatively computationally efficient and have been widely applied in assessments of impacts of regional climate change, particularly in hydrological response assessments (Chen et al., 2012; Hay and Clark, 2003). Thus, in this study, daily rainfall and meteorological variables were downscaled from monthly GCM simulations to specific sites with bias correction procedures using a statistical downscaling approach (Liu and Zuo, 2012) and this represents the first such application.

Downscaled climatic variables are adopted as the input data for hydrological models to simulate historical and future runoff and to estimate impacts of climate change on runoff (Chang and Jung, 2010; Ruelland et al., 2012). In this way, hydrological models are first calibrated using observed runoff data, and then the hydrological models are run using downscaled climatic data with the same calibrated parameters, and impacts of climate change on runoff are estimated using the modelled historical and future runoffs (Chiew et al., 2009; Reshmidevi et al., 2018). However, many uncertainties which depend on climate modelling, downscaling techniques and simulated hydrologic regimes, are incorporated along the entire modelling chain (Chen et al., 2012; Prudhomme et al., 2003). Climatic uncertainty is linked to Green House Gas (GHG) emission scenarios and especially to GCMs (Minville et al., 2008). Previous studies have suggested that choosing a single GCM is the main factor contributing to the overall uncertainty in climate change impact modelling (Jie et al., 2011; Wilby and Harris, 2006). Due to the enormous uncertainty caused by the choice of a single GCM, an ensemble of multiple GCMs has been adopted in many recent analyses (Tebaldi and Knutti, 2007; Zhang and Huang, 2013) and multi-GCMs ensembles appear to provide more comprehensive simulations of climatic variables than a single GCM (Knutti et al., 2010). In addition, using simulations of a multi-GCMs ensemble may balance out non-stationary biases, which is unlikely to be corrected by statistical downscaling approaches (Liu and Zuo, 2012). Therefore, a diversity of GCMs (28 from CMIP5 under RCP8.5) will be used in the present study to minimize the uncertainty caused by the choice of GCMs.

The Xinanjiang (XAJ) model, a rainfall-runoff basin model, has been successfully and widely used in humid and semi-humid catchments in China as a standard tool for a number of hydrological simulation purposes (Jayawardena and Zhou, 2000; Jiang et al., 2007; Xu and Singh, 2004; Yao et al., 2014). For example, Tian et al. (2013) used the XAJ model to assess impacts of climate change on river high-flows in a basin in China for the near future 2011–2040. It has also been successfully applied in many other countries including the United States, Canada, Germany, Belgium, France, Sweden, Japan and Thailand (Sahoo, 2005; Xu and Singh, 2004). For instance, Seiller and Anctil (2014) examined climate change impacts on the hydrologic regime of a catchment in Canada using the XAJ model and other lumped conceptual models. In addition, the XAJ model has been used across 210 catchments of southeast Australia, including the Murray–Darling basin and the south-east coast drainage basins that cover the most populated and important agricultural regions of Australia, with NSE values in the calibration periods of greater than 0.6 in 80 percent of these catchments (Li et al., 2009; Zhang and Chiew, 2009). Consequently, this study will apply the XAJ model forced with statistical downscaling of daily climate data based on 28 GCMs to study the hydrological response to climate change in an Australian catchment.

We aimed to evaluate hydrological responses to climate change in eastern Australia. Specifically, using the Manning River catchment as a case study, the objectives of this study were to: (1) test the performance of the XAJ model for simulating rainfall-runoff relationship of the Manning River catchment; (2) project future changes in simulated runoff, actual evapotranspiration and soil moisture content; and (3) identify the importance of different climatic variables in explaining future changes in water availability.

2. Materials and methods

2.1. Study area

The Manning River catchment is located on the New South Wales (NSW) mid north coast and includes the towns of Taree, Wingham, Gloucester and Walcha, and has a temperate climate with summer dominated rainfall (Chiew and Mcmahon, 2002) (Fig. 1). The catchment area is approximately 6630 km^2 with elevation ranging from 12 m to 1591 m (see Fig. 1). Mean annual temperature for the study area is 14.9 °C, mean annual rainfall is 1052 mm, mean annual potential evaporation is 1305 mm, and the runoff coefficient is 0.20 (Zhang et al., 2013). The Manning River flows for 250 km, rising in the Great Dividing Range to the east of the basin, and flowing south-east through a coastal floodplain to Taree where it divides in two. The Manning River catchment does not have large groundwater storages providing base flow to the river and the narrow floodplain pockets are the only source of base flow (Hughes et al., 2011). In addition, most of the rivers and creeks in the Manning River catchment are unregulated, with no major storages to capture and control flows. As in most unregulated rivers, flows are most affected during relatively dry times and this has been identified as one of the key water management issues in this catchment when water supply is low and consumptive demand high (https://www.industry.nsw.gov.au/water/basins-catchments/snapshots/manning). In addition, significant decreases in river flows, resulting from below average rainfall, affects the stability of the Manning river estuary entrance (Ruprecht and Peirson, 2011). However, very few studies regarding hydrological response to climate change have been

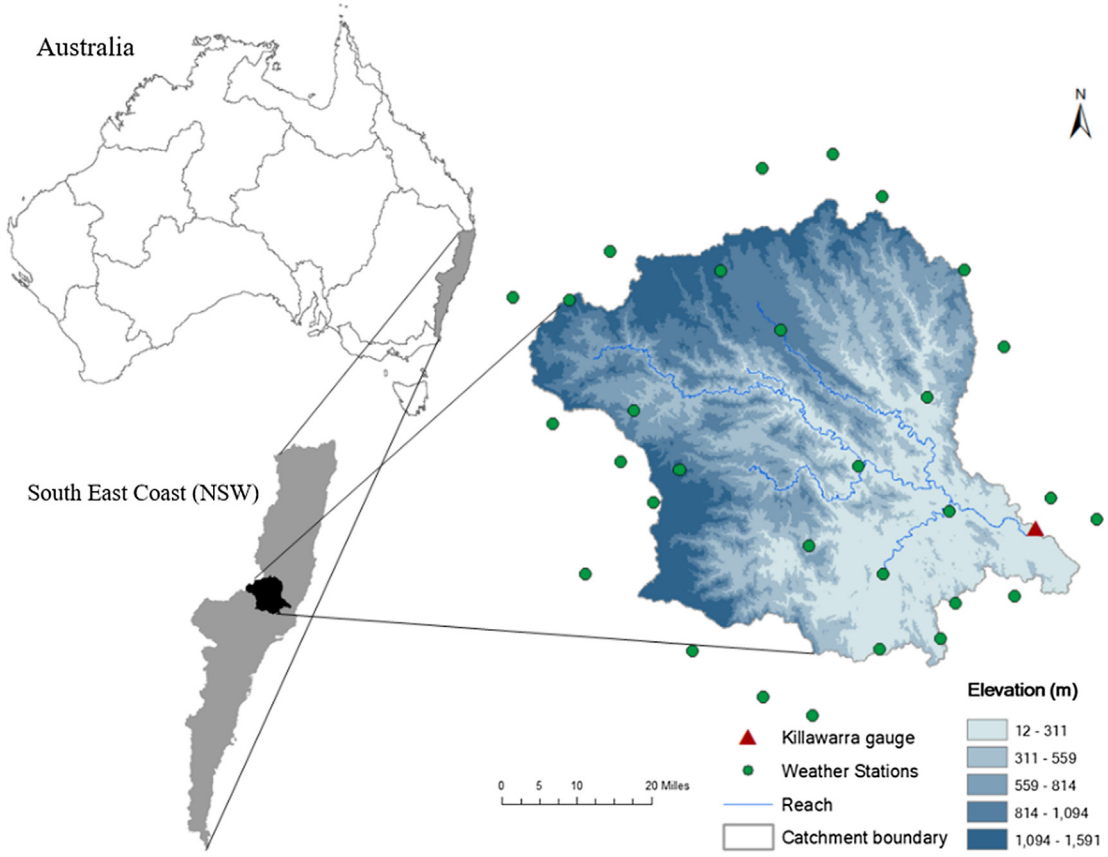

Fig. 1. The study area of Manning River catchment and location of observation stations including weather stations and gauge station.

carried out in the Manning River catchment. Thus, this study represents an important step toward the assessment of the effects of the changing climate on catchment runoff and can help inform future priorities for regional water management of river basin in the context of global climate change in eastern Australia. The Manning River gauging station at Killawarra receives streamflow from the vast majority of water sources within the Manning EMU (Entitlement Management Unit). Therefore, the Manning River catchment above Killawarra gauging station was selected as the case study area.

2.2. Observed data

Daily rainfall and potential evaporation data were used for hydrological simulation. To incorporate the large spatial heterogeneity of rainfall across this catchment, rainfall data from 30 meteorological stations sites within or close to the catchment were sampled (Fig. 1). The Thiessen polygon method was selected to estimate the mean area rainfall of this catchment because this is the most common and effective method for calculating spatial distribution of rainfall (Jiang et al., 2007). The method proposed by Abtew (1996) was used to calculate potential evapotranspiration (using solar radiation and maximum daily temperature) (Abtew, 1996). Daily streamflow data of the Killawarra hydrological station were collected from the website of the Australian Government Bureau of Meteorology (http://www.bom.gov.au/waterdata/). Daily observed hydrological and meteorological data in the period from 1991 to 2016 were used for hydrological model calibration and validation.

2.3. Statistical downscaling technique

Monthly gridded rainfall and climate data from GCMs were downscaled to the meteorological observation sites at a daily time step using a statistical downscaling model, NWAI-WG, developed by Liu and Zuo (2012). This rapid and reliable statistical downscaling method consists of two steps to perform spatial and temporal downscaling separately. This approach relies on empirical relationships between observational data and GCM outputs. First, the monthly gridded climate projections from GCMs were spatially interpolated to specific sites of interest (in this case 30 sites within or close to the Manning river catchment, Fig. 1) using an inverse distance-weighted (IDW) interpolation method, followed by a bias correction procedure to correct site-based monthly GCM simulations. Second, daily climatic variables (e.g. maximum and minimum temperatures and rainfall) were then generated for each site from the spatially downscaled projections by using a modified version of the WGEN stochastic weather generator (Richardson and Wright, 1984) with parameters derived from the bias-corrected monthly data (see Liu and Zuo 2012 for details). The validation carried out by Liu and Zuo (2012) has shown that this downscaling method can reproduce the observed climatic variables at daily, monthly and annual time-scales well. Unlike other statistical downscaling approaches developed in Australia, which have only been applied to either specific time periods (Timbal et al., 2009) or small areas (Mehrotra and Sharma, 2010) due to data availability or time and cost, this approach can be easily applied to any archived monthly GCM data for any site and across multiple time periods as the approach requires only monthly GCM data and daily historical climate records. In this research, we applied a post downscaling treatment to the NWAI-WG downscaled data. When the downscaled site climate data are applied to catchment, the occurrence of inconsistent daily rainfalls between sites can result in a) more rainfall days and b) smaller daily rainfall over the catchment and potentially poor simulation of the peak flows. In the post downscaling treatment, we selected the central station as the reference station and re-downscaled other 29 sites in the catchment to have the same rainfall events with the amounts of GCM projected rainfalls for respective sites. This

method is validate based on the hypothesis that the weather stations are close enough so that the rain days are fairly consistent. The catchment area is approximately 6630 km^2, that is, the radius of the study area is around 40 km. Thus, we considered this catchment downscaling method is validate for this study.

This study was focused on the analyses of three periods of simulations: the first examined the period 1977–2016 (referred to as 'immediate past' or 'baseline'), the second examined the period 2021–2060 (referred to as 'the near future' or '2040 s'), and the third the period 2061–2100 (referred to as 'the far future' or '2080 s'). In addition, for baseline and future time periods, hydro-meteorological variables were downscaled from 28 GCMs (Wang et al., 2017) of the Coupled Model Intercomparison Project 5 (CMIP5) under the RCP8.5 scenario. RCP 8.5, a scenario that represents comparatively high greenhouse gas emission (Riahi et al., 2011) and matches the current trajectory of GHGs (Fuss et al., 2015; Pagán et al., 2016). To present the range in projected future climate, monthly, seasonal and annual change in maximum and minimum temperatures and rainfall for the 28 GCMs in the near future and the far future compared to baseline were computed for the catchment. In addition, monthly, seasonal and annual changes in runoff, evapotranspiration and soil moisture for the 28 GCMs in the 2040 s and 2080 s compared to baseline were estimated to show the range in projected future hydrological variables.

2.4. The XAJ model

The XAJ model is a lumped conceptual rainfall–runoff model with physical-based parameters (Zhao et al., 1980). The model is widely used in humid and semi-humid basins in China (Hu et al., 2005), and was recently adopted and validated in southeast Australia (Li et al., 2012). Furthermore, the XAJ model consistently performs better than four other conceptual rainfall-runoff models (the Pitman model of South Africa (Hughes, 2013), the Sacramento model of USA (Sorooshian et al., 1993), the NAM model of Denmark (Nielsen and Hansen, 1973) and the SMAR model of Ireland (Kachroo, 1992)) even in relatively dry catchments (Gan et al., 1997). Therefore, the XAJ model was selected for hydrological simulations in the present study. The XAJ model, which uses rainfall and potential evapotranspiration data to simulate runoff, actual evapotranspiration and soil moisture content, is divided into four layers: evapotranspiration, runoff production, separation of runoff components and flow concentration (Zhao, 1992). Its main feature is the concept of runoff formation of repletion of storage, which means that runoff is not produced until the soil moisture content of the aeration zone reaches field capacity, and thereafter runoff equals the rainfall excess without further loss (Zhao, 1992). The flow chart of the XAJ model is shown in Fig. 2 and the model parameters are listed in Table 1. It should be noted that the XAJ model used in this study does not consider vegetation and its interaction with the atmosphere. However, it has the advantage of fewer input data and simpler application.

It is crucial for water resource managers to be conscious of and prepared for the impacts of climate change on hydrological variables. Therefore, daily hydrological simulations under baseline and future scenarios were obtained using the XAJ model driven by downscaled climatic variables from 28 GCMs to evaluate the changes in catchment hydrological cycle. Runoff, which represents an integrated response to climatic inputs throughout the whole drainage basin, is a very important indicator of the impacts of climate change on water resources. In addition, climate change will lead to changes in other hydrological variables which can also be simulated by the XAJ model. Therefore, changes of actual evapotranspiration and soil moisture content were also included in this study. Soil moisture is defined as the areal mean tension water storage (W) in the XAJ model (Zhao, 1992). The XAJ model was calibrated and validated against river flow data only. We did not calibrate and validate the model simulations in actual evapotranspiration and soil moisture content because of a lack of field data for these variables. The absolute values of soil moisture content should therefore not be used directly. Nevertheless, it is still reasonable and valuable to compare the relative changes in the simulations because the model mimics the actual hydrological processes.

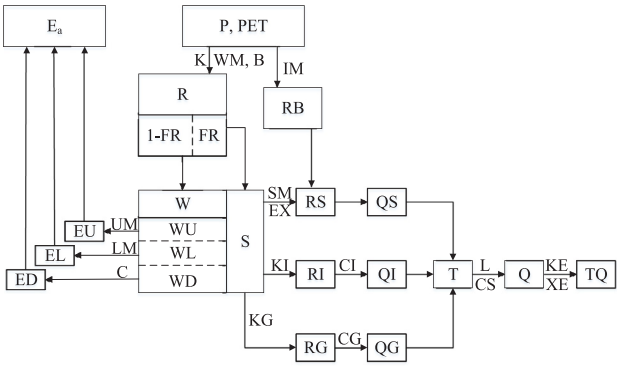

Fig. 2. Flow chart for the XAJ model. The inputs to the model are P (rainfall) and PET (potential evapotranspiration), the outputs are Ea (the actual evapotranspiration from the whole catchment, which is the sum of the evapotranspiration from the upper soil layer EU, the lower soil layer EL, and the deepest layer ED) and TQ (the outlet discharge from the whole catchment), and W (area mean tension water storage, namely soil moisture, which is the sum of WU, WL and WD in the upper, lower and deepest layer). The meanings for the state variables and parameters appear inside and outside of the blocks in this figure can be found in Table 1 and the reference (Zhao, 1992).

2.5. Parameter estimation and performance evaluation

There are a lot of missed observed flow data in 1983, 1989 and 1990 at Killawarra gauging station. However, observed flow data from 1991 to 2016 (26 years) are relatively complete and continuous and were selected for model calibration and validation. The time period for calibration and validation years was determined by the length of the observed data record. For sufficiently long periods of observed data that represent different climate conditions, it is possible to split the available data equally for calibration and validation. However, the observed record (26 years) is not sufficient for an equal split, the length of the data may be different in such a way that the calibration period is sufficiently long since optimized model parameters during calibration are used for model validation without further adjustment (Ayele et al., 2017). Therefore, daily observed and simulated runoff in the period 1991–2008 (18 years) were used for model calibration and data from 2009 to 2016 (8 years) were used for model validation. A global optimization method, the SCE-UA (shuffled complex evolution method developed at the University of Arizona) (Duan et al., 2015), is an effective and efficient optimization technique for calibration of watershed models and was used to optimize XAJ model parameters. It combines the best features of "multiple complex shuffling" and "competitive evolution" based on the simplex search method (Nelder and Mead, 1965). The XAJ model is calibrated by maximizing the Nash-Sutcliffe Efficiency (NSE) (Nash and Sutcliffe, 1970) of daily flow together with a constraint to ensure that the total modelled flow in the calibration period is within 5% of the total observed flow (Vaze and Teng, 2011). NSE and coefficient of determination (R^2) were used to evaluate the performance of the XAJ model. The NSE is one of the most widely used criteria for comparing hydrologic model performance with observed values (Le and Pricope, 2017). In addition, many studies also used NSE and R^2 to evaluate the performance of hydrological models (Le and Pricope, 2017; Vu et al., 2012). NSE varies from $-\infty$ to 1. A value of 1 means the simulations perfectly match the observations, so the closer the NSE value is to 1, the better the hydrological model is deemed to have performed. In general, when both NSE and R^2 exceed 0.50, the hydrological model is deemed to effectively simulate stream flow for a

Table 1
16 calibrated parameters for the XAJ model in Manning River catchment.

Layers	Parameters	Meaning of parameters (units)	Values
Evapotranspiration	UM	Areal mean tension water capacity in the upper layer (mm)	28
	LM	Areal mean tension water capacity in the lower layer (mm)	90
	C	Coefficient of deep evapotranspiration	0.023
Runoff production	WM	Areal mean tension water capacity (mm)	137
	B	Exponent of the tension water capacity curve	0.1
	IM	Ratio of the impervious to the total area of the basin	0.001
Separation of runoff components	SM	Areal mean of the free water capacity of the surface soil layer (mm)	27
	EX	Exponent of the free water capacity curve	0.97
	KG	Outflow coefficient of the free water storage to groundwater	0.52
	KI	Outflow coefficient of the free water storage to interflow	0.26
Flow concentration	CI	Recession constant of the interflow storage	0.78
	CG	Recession constant of groundwater storage	0.996
	CS	Recession constant of surface water storage	0.38
	L	Lag time (day)	0
	KE	Parameters of the Muskingum method (h)	24
	XE	Parameters of the Muskingum method	0.43

given catchment (Liu et al., 2017). The NSE and R^2 were calculated as follows:

$$NSE = 1 - \frac{\sum_{i=1}^{N}(Q_{obs,i} - Q_{sim,i})^2}{\sum_{i=1}^{N}(Q_{obs,i} - \bar{Q}_{obs})^2} \quad (1)$$

$$R^2 = \frac{[\sum_{i=1}^{N}(Q_{obs,i} - \bar{Q}_{obs})(Q_{sim,i} - \bar{Q}_{sim})]^2}{\sum_{i=1}^{N}(Q_{obs,i} - \bar{Q}_{obs})^2 \sum_{i=1}^{N}(Q_{sim,i} - \bar{Q}_{sim})^2} \quad (2)$$

where Q_{obs} and Q_{sim} are the observed and simulated daily flow (m^3/s) respectively, $\bar{Q}$ is the mean flow (m^3/s), i is the ith sample, and N is the number of samples.

2.6. Regression analyses

Prior to the analysis of the simulations we applied a bias-correction procedure, called secondary bias correction (Yang et al., 2016) to correct the differences of the simulated outputs forced by GCM projected climate over those forced by observed climate.

A multiple Liner Regression Model (MLRM) was used to quantify the effects of climate variables (maximum and minimum temperatures and rainfall) on hydrologic variables (runoff, evapotranspiration and soil moisture). MLRM is a linear model that describes how y-variable relates to two or more x-variables (Dar, 2017). The general structure of the model is as given below:

$$Y = \beta_0 + \beta_1 X_1 + \beta_2 X_2 + \ldots \quad (3)$$

where, y is the dependent (or response) variable, x is independent (or predictor) variable.

In this study, the model is defined as below:

$$\Delta Y = a\Delta T_{max} + b\Delta T_{min} + c\Delta R \quad (4)$$

where ΔY (%) is projected changes in hydrological variables (runoff, actual evapotranspiration or soil moisture), ΔT_{max} (°C), ΔT_{min} (°C) and ΔR (%) are changes in maximum and minimum temperatures and rainfall, respectively. From these regression analyses, the contribution of the change in specific climate factors to changes in hydrologic variables were quantified. In addition, rainfall elasticity (c, defined here as the proportional change in runoff divided by the proportional change in rainfall) can also be derived.

3. Results

3.1. XAJ model calibration and validation

Calibrated parameters for the XAJ model in the Manning River catchment are shown in Table 1. Runoff simulations at daily time scale were aggregated to monthly values, and were compared with the observed data. Monthly observed runoff and the XAJ model simulated runoff for calibration and validation periods in the Manning River catchment were strongly correlated ($R^2 \geq 0.94$ and NSE ≥ 0.92) and closely replicated temporal variation (Figs. 3 and 4), with slopes within 25% of the 1:1 regression. The slope of the regression during the validation period was much closer to the 1:1 line than that in the calibration period, which may be caused by the slight underestimation of the extremely high runoff observed in the calibration period.

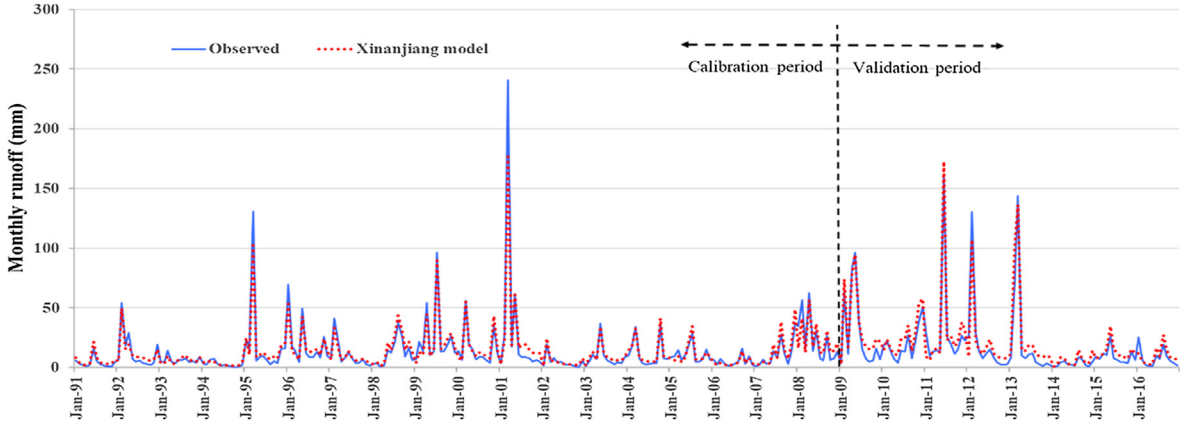

Fig. 3. The observed and simulated monthly runoff during calibration (1991–2008) and validation periods (2009–2016) in the Manning River catchment.

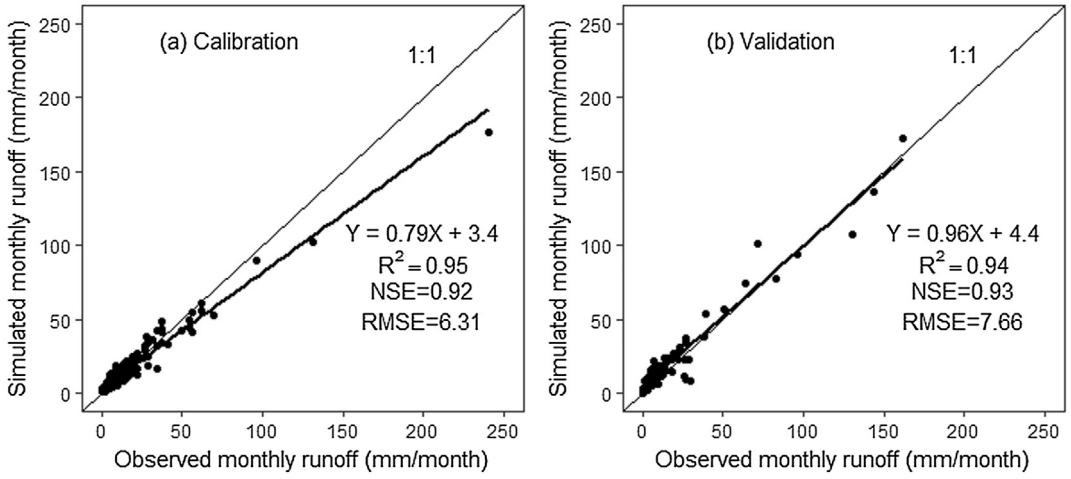

Fig. 4. Comparison of observed and simulated monthly runoff during (a) calibration and (b) validation periods.

3.2. Projected changes in temperature and rainfall

Projected maximum and minimum temperatures and rainfall in the future were aggregated to monthly and seasonal time scales, and compared with baseline values. All 28 GCMs used in this study agree on a future temperature rise, with higher temperature increases in 2080 s than 2040 s at both monthly and seasonal time-scales (Figs. 5 and 6). For maximum monthly temperatures (Fig. 5a), the largest median increase was 1.6 °C (0.9–1.9 °C) in November by 2040 s and 3.8 °C (3.5–4.2 °C) in September by 2080 s, while the lowest median increase was 1.1 °C (0.9–1.7 °C) in March by 2040 s and 2.5 °C (1.8–3.0 °C) in February by 2080 s. The range of uncertainty in brackets indicates the 25th and 75th percentiles of the 28 GCMs used herein. At seasonal time-scales (Fig. 6a), the maximum temperature was projected to increase most in spring in both future periods (the median increase was 1.5 °C (1.1–1.8 °C) in 2040 s and 3.4 °C (2.8–3.9 °C) in 2080 s), while increases were lowest in autumn in 2040 s (1.3 °C (0.9–1.6 °C)) and in summer in 2080 s (2.9 °C (2.4–3.4 °C)). For temperature minima (Figs. 5b and 6b), the median estimate demonstrated the largest increase in May (1.9 °C (1.6–2.5 °C) in 2040 s and 4.9 °C (3.7–5.5 °C) in 2080 s) (autumn (1.7 °C (1.4–1.9 °C) in 2040 s and 4.1 °C (3.3–4.7 °C) in 2080 s) and the smallest increase in temperature minima in February (1.0 °C (0.8–1.3 °C) in 2040 s and 2.5 °C (1.8–3.1 °C)) in 2080 s (summer (1.2 °C (0.9–1.3 °C) in 2040 s and 2.7 °C (2.3–3.2 °C) in 2080 s)) in the future. The median increase for maximum temperature at an annual time-scale was 1.4 °C (1.2–1.5 °C) by 2021–2060 and 3.2 °C (2.7–3.5 °C) by 2061–2100 (Fig. 6a), while median annual minimum temperatures were predicted to increase by 1.5 °C (1.3–1.7 °C) in 2040 s and 3.5 °C (3.1–4.1 °C) in 2080 s (Fig. 6b).

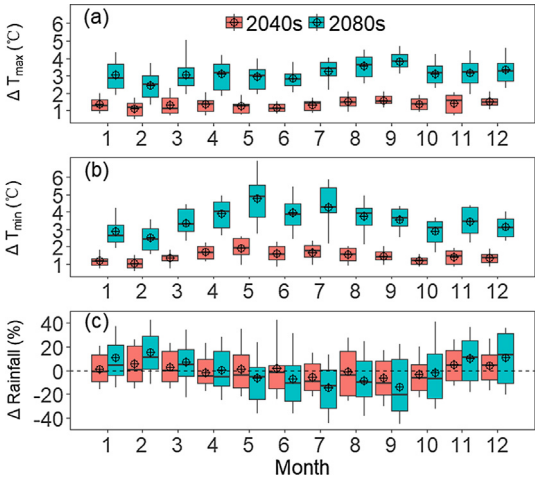

Fig. 5. Projected changes in maximum temperature (T_{max}) (°C), minimum temperature (T_{min}) (°C) and rainfall (%) in the near future (2021–2060, 2040 s) and the far future (2061–2100, 2080 s) under RCP8.5 based on 28 GCMs compared with baseline at monthly time scale. Data presented are changes in the 40-year mean values for each of the 28 GCMs. Box boundaries indicate the 25th and 75th percentiles; the black lines and crosshairs within the box mark the median and mean, respectively; the lower and upper whiskers indicate the 10th and 90th percentiles.

Changes to future rainfall differ across the different GCMs and across seasons, with the majority of GCMs simulating increases in November-March rainfall and the majority of GCMs simulating decreases in the period of April to October. The largest ensemble median increase in rainfall occurred in December (4.2% (−7.6–13.4%) in 2040 s and 13.4% (−10.9–31.4%) in 2080 s), while the largest median decrease occurred in September (−10.6% (−20.7–8.1%) in 2040 s and −20.7% (−34.0–9.7%) in 2080 s) (Fig. 5c). Median spring (−1.7% (−13.5–10.0%) in 2040 s and 1.4% (−17.4–13.8%) in 2080 s) and autumn (−1.1% (−6.0–4.8%) in 2040 s and 0.7% (−9.3–7.5%) in 2080 s) rainfall was projected to have relatively small changes in the future. In contrast, median rainfall was projected to have a larger increase in summer (4.2% (−3.6–11.7%) in 2040 s and 9.1% (−2.9–24.9%) in 2080 s) but a decline (−4.0% (−13.1–3.1%) in 2040 s and −11.7% (−20.9–3.5%) in 2080 s) in winter, with larger changes in 2080 s than in 2040 s. At annual time-scales, the changes in rainfall, as estimated by the 28, ranged from −5.2% (25th percentile) to 4.2% (75th percentile) in 2040 s and −9.5% (25th percentile) to 10.8% (75th percentile) in 2080 s with ensemble median values of −0.3% and 4.6%, respectively.

3.3. Changes in simulated runoff, actual evapotranspiration and soil moisture

Projected runoff, evapotranspiration and soil moisture content were aggregated to monthly and seasonal time-scales, and were compared with baseline data. The largest median monthly increase in runoff was 6.9% (−23.2–26.7%) in November by 2040 s and 31.1% (−2.6–71.4%) in February by 2080 s, while the largest median decrease was −16.7% (−23.9–13.2%) in June by 2040 s and −20.5% (−31.1–4.2%) in July by 2080 s (Fig. 7a). Thus, the largest monthly runoff is projected to shift from March (during the baseline period; Table 2) to February in the far future. The lowest runoff in September was simulated to decline (−4.3% (−24.2–14.3%) in 2040 s and −16.3% (−33.2–3.8%) in 2080 s) in the future. The second largest runoff, which occurred in the summer in the baseline period, was projected to increase (11.6% (−12.8–24.9%) in 2040 s and 23.8%

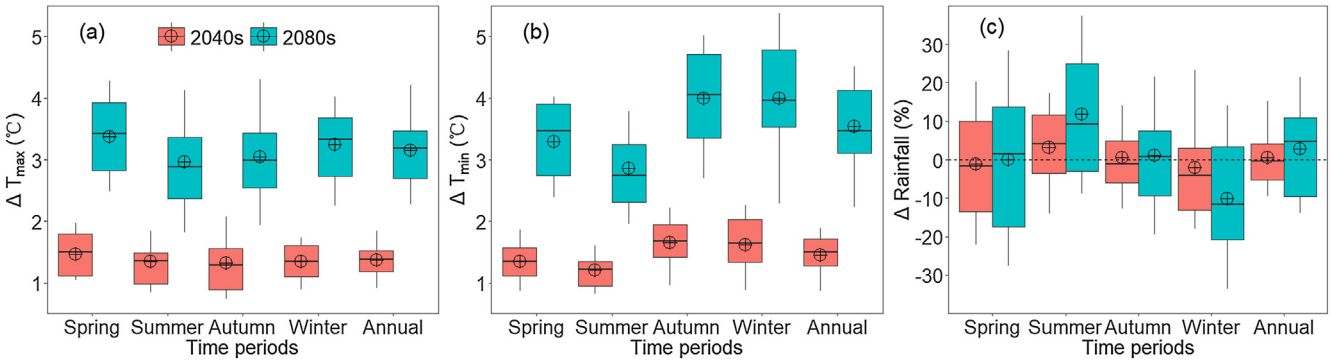

Fig. 6. Projected changes in maximum temperature (T_{max}) (°C), minimum temperature (T_{min}) (°C) and rainfall (%) in the near future (2021–2060, 2040 s) and the far future (2061–2100, 2080 s) under RCP8.5 based on 28 GCMs compared with baseline at seasonal and annual time scales. Data presented are changes in the 40-year mean values for each of the 28 GCMs. Box boundaries indicate the 25th and 75th percentiles; the black lines and crosshairs within the box mark the median and mean, respectively; the lower and upper whiskers indicate the 10th and 90th percentiles.

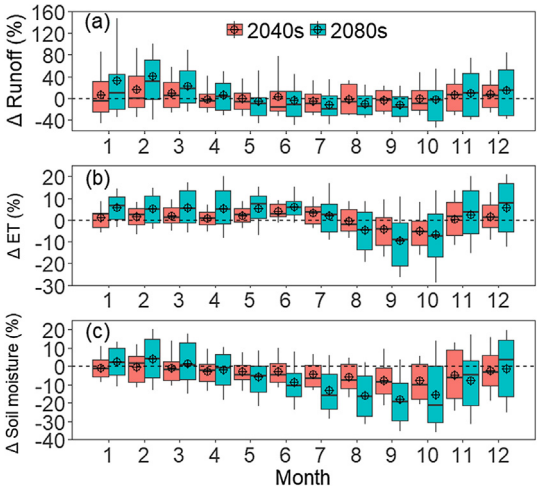

Fig. 7. Projected changes in runoff (%), actual evapotranspiration (%) and soil moisture (%) in the near future (2021–2060, 2040 s) and the far future (2061–2100, 2080 s) under RCP8.5 based on 28 GCMs compared with baseline at monthly time scale. Data presented are changes in the 40-year mean values for each of the 28 GCMs. Box boundaries indicate the 25th and 75th percentiles; the black lines and crosshairs within the box mark the median and mean, respectively; the lower and upper whiskers indicate the 10th and 90th percentiles.

Table 2
Mean values in climatic and simulated hydrological variables in the baseline period (1977–2016) in Manning River catchment.

Time periods	T_{max} (°C)	T_{min} (°C)	Rainfall (mm)	Runoff (mm)	Actual Evapotranspiration (mm)	Soil moisture content (mm)
January	26.3	14.7	154.7	18.0	100.3	65.7
February	25.6	14.6	144.1	27.0	90.7	79.5
March	24.3	13.0	125.3	28.1	86.5	82.0
April	21.3	9.8	74.4	18.2	60.8	77.7
May	17.4	6.9	77.5	19.2	46.1	79.9
June	14.4	4.6	73.5	19.5	39.4	88.8
July	13.7	3.1	53.9	17.0	43.6	89.4
August	15.3	3.7	55.1	15.6	51.9	80.3
September	18.3	5.8	55.2	11.9	60.1	67.8
October	21.2	8.7	84.8	14.1	74.3	60.9
November	23.5	11.0	91.5	12.7	82.1	58.3
December	25.6	13.2	110.0	13.8	94.9	58.5
Spring	21.0	8.5	231.5	38.6	216.5	62.4
Summer	25.9	14.2	408.8	58.8	286.0	67.9
Autumn	21.0	9.9	277.2	65.5	193.4	79.9
Winter	14.5	3.8	182.5	52.1	135.0	86.2
Annual	20.6	9.1	1100.0	214.9	830.9	74.1

(−5.3–46.2%) in 2080 s) in the future, whereas the second smallest runoff, which currently occurs in winter, was projected to decline (−6.9% (−23.0–4.9%) in 2040 s and −14.8% (−28.7 to −0.06%) in 2080 s) in the future (Table 2, Fig. 8a). Thus, the largest seasonal runoff which currently occurs in the autumn was predicted to change to the summer in 2040 s and 2080 s. In addition, in 2080 s, these monthly and seasonal changes generally became larger than those predicted in the 2040 s (Figs. 7a and 8a). There were considerable differences in the runoff projection of different GCMs (Figs. 7a, 8a). Thus, at annual time-scales, runoff change estimated by the 28 GCMs ranged from −10.6% (25th percentile) to 8.9% (75th percentile) in 2040 s and −17.2% (25th percentile) to 22.0% (75th percentile) in 2080 s with median values of −2.3% and 7.7%, respectively (Fig. 8a). Furthermore, median values in annual runoff in 2080 s showed a slight increase compared to 2040 s (Fig. 8a) and this may be related to the increase in rainfall in 2080 s (Fig. 6c).

There was a wide range in differences among modelled values of actual evapotranspiration responses simulated by the 28 GCMs. Median monthly actual evapotranspiration was projected to decrease only in August (−2.2% (−5.1–5.1%) in 2040 s and −4.3% (−13.7–3.7%) in 2080 s), September (−4.1% (−11.4–1.3%) in 2040 s and −8.9% (−21.1 to −1.4%) in 2080 s) and October (−5.3% (−11.7 to −0.4%) in 2040 s and −7.4% (−16.9–3.0%) in 2080 s) (winter/spring), while median seasonal actual evapotranspiration only showed a trend of decreasing values (−2.2% (−10.3–2.7%) in 2040 s and −3.2% (−15.7–3.7%) in 2080 s) in spring in the future (Figs. 7 and 8). At annual time-scales, actual evapotranspiration change estimated by the 28 GCMs ranged from −3.0% (25th percentile) to 3.7% (75th percentile) in 2040 s and −4.3% (25th percentile) to 8.6% (75th percentile) in 2080 s with median values of 0.6% and 1.8% respectively (Fig. 8b). However, the differences in actual evapotranspiration changes under different GCMs are smaller than the modelled changes in runoff (Figs. 7a, b and 8a, b). Differences in predicted 40-year mean monthly, seasonal and annual soil moisture content resulting from different GCMs were also considerable (Figs. 7c, 8c). Furthermore, the median estimate indicated that monthly soil moisture content was projected to have a trend of decreasing values (except February (1.5% (−8.8–5.3%))) in 2040 s and to increase slightly only in December (3.6% (−16.6–14.1%)), January (2.0% (−5.0–9.7%)), February (4.1% (−6.2–14.9%)) and March (0.7% (−7.0–12.9%)) in 2080 s, while seasonal soil moisture was predicted to decrease in 2040 s and to increase marginally (0.5% (−7.9–10.7%)) only in summer in 2080 s. Finally, at annual time-scales, changes in soil moisture content simulated by the 28 GCMs ranged from −8.8% (25th percentile) to 0.2% (75th percentile) in 2040 s and −15.5% (25th percentile) to −1.6% (75th percentile) in 2080 s with ensemble median values of −4.4% and

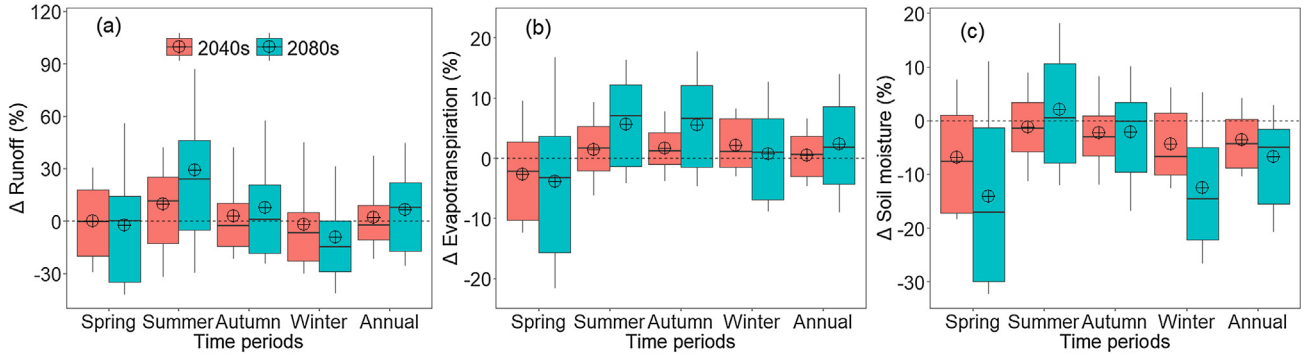

Fig. 8. Projected changes in runoff (%), actual evapotranspiration (%) and soil moisture (%) in the near future (2021–2060, 2040 s) and the far future (2061–2100, 2080 s) under RCP8.5 based on 28 GCMs compared with baseline at seasonal and annual time scales. Data presented are changes in the 40-year mean values for each of the 28 GCMs. Box boundaries indicate the 25th and 75th percentiles; the black lines and crosshairs within the box mark the median and mean, respectively; the lower and upper whiskers indicate the 10th and 90th percentiles.

−5.1% respectively.

3.4. Relationships among hydrological responses and climate variables

Relationships among changes in hydrologic variables (runoff, evapotranspiration and soil moisture content) and changes in daily maximum and minimum temperatures and rainfall are shown in Table 3. Runoff, actual evapotranspiration and soil moisture content were all largely dominated by rainfall at annual and seasonal time-scales. At annual time-scales, change in runoff was only significantly correlated with change in rainfall, while change in actual evapotranspiration was significantly correlated with change in rainfall, and daily maximum and minimum temperatures, while soil moisture content was primarily dominated by rainfall and daily maximum temperature. Furthermore, correlations of changes in hydrological variables to changes in climatic variables were estimated using the multiple regression model. For example, runoff could change by 5.1, 7.2, −7.7 and −10.6% in spring, summer, autumn and winter, respectively, with an annual change of −4.9%, as a result of an increase of maximum temperature of 1.0 °C. Annual rainfall elasticity of runoff was about 2.1, that is, a 1% change in mean annual rainfall results in a 2.1% change in mean annual runoff in this catchment. Finally, the effect of changes in rainfall on actual evapotranspiration was smaller than its effect on soil moisture content, and much smaller than its impact on runoff at seasonal and annual time-scales. For instance, a 1% change in mean annual rainfall results in a 0.6% and 0.8% change in mean annual actual evapotranspiration and soil moisture content, respectively, in this catchment.

Table 3
Regression coefficients of projected changes in hydrological variables (ΔY, %) including runoff, actual evapotranspiration and soil moisture with changes in daily maximum temperature (ΔT_{max}, °C), daily minimum temperature (ΔT_{min}, °C) and rainfall (ΔR, %) in a multiple linear regression model ($\Delta Y = a\Delta T_{max} + b\Delta T_{min} + c\Delta R$); *p < 0.05, **p < 0.01, ***p < 0.001.

Hydrologic variables	Time periods	a	b	c	Adjusted R^2
Δ Runoff	Annual	−4.89	4.50	2.08***	0.85
	Spring	5.10	−5.50	1.46***	0.72
	Summer	7.19*	−8.99*	2.69***	0.89
	Autumn	−7.73***	7.37***	1.84***	0.87
	Winter	−10.62*	10.28**	1.61***	0.77
Δ Actual evapotranspiration	Annual	1.50*	−1.11*	0.55***	0.88
	Spring	−2.98*	1.94	0.58***	0.85
	Summer	1.67*	−1.22	0.37***	0.82
	Autumn	1.06	0.56	0.25***	0.53
	Winter	−0.35	1.61	0.37***	0.64
Δ Soil moisture	Annual	−1.64*	−1.08	0.76***	0.90
	Spring	−3.84*	−0.23	0.68***	0.88
	Summer	−0.05	−1.83*	0.62***	0.88
	Autumn	−3.69**	2.11*	0.52***	0.67
	Winter	−4.24*	1.82	0.55***	0.80

4. Discussion

In this study, hydrological responses to climate change in the Manning River catchment were simulated using an ensemble of 28 GCMs and the XAJ model. The overall calibration and validation results demonstrated that the XAJ model was able to satisfactorily reproduce the observed runoff in this catchment (Figs. 3 and 4), and the calibrated XAJ model can be further used to evaluate the impacts of climate change on catchment hydrological variables. While the hydrological model was generally able to replicate observed runoff, it might have some difficulties in reproducing the extreme high runoff in the calibration period (Figs. 3 and 4). Similar results in reproducing peak flow also occur in other hydrological models. For example, Tian et al. (2013) used three models (GR4J (Perrin et al., 2003), HBV (Lindström et al., 1997) and XAJ) to simulate daily discharge and their results demonstrated an underestimation of high rates of discharge in all three models. Eum et al. (2017) used the Variable Infiltration Capacity (VIC) hydrologic model to simulate daily runoff and found a poor capacity to simulate both low flows and very high flows. Thus, difficulties in reproducing the highest rates of runoff are common because of the theories of hydrological models and criteria of model calibration. This may be attributed to the theory of runoff production (Hao et al., 2015). For example, the XAJ model assumes that runoff is not generated until soil moisture content of the aeration zone reaches field capacity. This assumption may not be valid during heavy rain events because these can produce runoff when soils are not fully filled with water (unsaturation runoff) due to insufficient infiltration, which is not simulated in the XAJ model (only saturation excess runoff is simulated). Therefore, modification of the model structure by including unsaturation runoff during heavy rainfall events may lead to improved hydrologic simulations during these periods.

Our results indicated that the median annual increase for maximum temperature was 1.4 °C (1.2–1.5 °C) by 2021–2060 and 3.2 °C (2.7–3.5 °C) by 2061–2100, while minimum temperature was predicted to increase by 1.5 °C (1.3–1.7 °C) in 2021–2060 and 3.5 °C (3.1–4.1 °C) in 2061–2100. The projected trend of increasing temperature agrees with previous studies. For instance, Wang et al. (2017) reported a 3.7 °C increase in temperature for RCP8.5 across the wheat belt in NSW by 2061–2100. Moreover, an ensemble of 12 RCM simulations (4 GCMs × 3 RCMs) performed by the NSW and ACT Regional Climate Modelling (NARCliM) project projects a 0.7 °C rise in mean temperature by 2020–2039 and a 2.0 °C rise by 2060–2079 in the north coast region of NSW (including the Manning River catchment) (www.ccrc.unsw.edu.au/sites/default/files/NARCliM/index.html). However, it should be

noted that future time periods in our research (2021–2060 and 2061–2100) and the NARCliM project (2020–2039 and 2060–2079) are not exactly the same. In addition to temperature, our results also showed that median rainfall is projected to have a significant increase in summer and a decrease in winter in the future, although the largest rainfall is in the summer and the lowest rainfall is in winter in this catchment (Table 2). Therefore, the trend of increasing values in high rainfalls and a trend of decreasing values in low rainfalls are likely to generate a larger degree of inter-seasonal variation in the Manning River catchment in the future. This is generally consistent with previous studies. For example, NARCliM also projects an increase in rainfall during summer, autumn and spring and a decrease in winter across the north coast region by 2060–2079. In addition, Liu and Zuo (2012) analyzed the changes in summer and winter rainfall and found an increase in summer rainfall, whilst winter rainfall has a high probability of decreasing in most areas of New South Wales.

Our results showed that multi-GCM ensemble median values exhibit a slight decrease (−2.3% (−10.6–8.9%)) in annual runoff in 2040 s, which is similar to the trend of change in previous studies, despite the GCMs, hydrological models, downscaling methods and time periods differing across studies. For instance, Chiew and Mcmahon (2002) concluded that the annual runoff in catchments on the east coast of Australia could change by ±15% by 2030 relative to 1990. Similarly, Chiew et al. (2003) used the SIMHYD model and the CSIRO Mark 2 GCM simulations and found a decrease in mean annual runoff of 6–8% in most of eastern Australia in 2021–2050 relative to 1961–1990. Vaze and Teng (2011) used 15 GCMs and the median estimate indicates that future mean annual runoff in 2030 relative to 1990 will be no change to a slight reduction in the eastern parts of Australia. In addition, median estimates suggest a trend of increasing values in summer runoff (the second largest runoff in the baseline period) and a trend of decreasing values in winter runoff (the second smallest runoff in the baseline period) in the future. Consequently, the trend of increasing values of high runoffs and a trend of decreasing values of low runoffs is likely to generate larger inter-seasonal differences in the future. This seasonal change in runoff is also consistent with previous studies (Chiew et al., 2009; Eisner et al., 2017; Vaze and Teng, 2011). Moreover, median estimates show that seasonal soil moisture content is predicted to decrease significantly in spring and winter. The projected decrease in runoff and soil moisture in winter will threaten surface water supplies and have adverse implications for agriculture (Gardner, 2009), which has significant implication for land and water resource management in the future.

Changes in regional temperature and rainfall expected to occur as a result of future climate change may have significant impacts on different components of a catchment water budget (Nash and Gleick, 1991). Thus, changes in runoff are largely related to variations in rainfall (Reshmidevi et al., 2018). In addition, changes in temperature are likely to have impacts on runoff production through increasing evapotranspiration from soil and vegetation (Wang et al., 2016). Our results suggested that runoff changes are more sensitive to changes in rainfall than changes to temperature (Table 3) and this agrees with previous studies (Chiew et al., 1995). A case in point is that Chiew and Mcmahon (2002) carried out climate change impacts modelling on 28 unimpaired Australian catchments and found that the impact on runoff was much more dependent on rainfall than temperature. Rainfall elasticity is a simple estimate of the sensitivity of runoff to changes in rainfall, and is particularly useful as an initial estimate of climate change impacts on runoff (Chiew, 2006). Thus, it should be noted from Table 3 (coefficient "c" for annual runoff is 2.08) that the percentage change in average annual rainfall is generally amplified two fold in average annual runoff change, which is also in commonly observed in previous research (Chiew, 2006; Sankarasubramanian et al., 2001). For example, Jones et al. (2006) estimated the sensitivity of mean annual runoff to climate change using 3 models across 22 Australian catchments and results show mean sensitivities of 2.4%, 2.5% and 2.1% change in mean annual flow for every 1% change in mean annual rainfall, respectively. In addition, Table 3 shows that the lowest seasonal rainfall elasticity of runoff was observed in spring, and this may be because of the largest ET/P (Evapotranspiration/Rainfall) ratio occurring in spring (Table 2), which means spring is a relatively dry season in this catchment, and the increase in rainfall is mainly used to evaporate and replenish soil moisture content (Table 3 shows that the highest value of coefficient "c" for seasonal actual evapotranspiration and soil moisture occurs in spring).

In addition to runoff, variation in modelled actual evapotranspiration and modelled soil moisture content were also both largely dominated by variation in rainfall and have a weaker correlation with changes in temperature at annual and seasonal scales (Table 3). Therefore, there was a good correlation between the major components of the water budget and rainfall, reflecting the fact that rainfall is the ultimate source of water for the land surface water budget (Fekete et al., 2004). However, the effect of variation in rainfall on actual evapotranspiration is much smaller than its effect on runoff, in agreement with previous findings (Chiew and Mcmahon, 2002).

Assessments of the impacts of climate change on catchment water budgets are affected by the uncertainties in the GCMs, downscaling methods and GHG emission scenarios, as well as the uncertainty in the hydrologic model itself. This study used an ensemble of 28 GCMs to reduce uncertainties arising from the choice of a single GCM. However, we only used one hydrological model to simulate water resource availability, and therefore this may contribute some uncertainty because of the choice of model parameters and model structure (Eum et al., 2017). Jiang et al. (2007) applied six, monthly water balance models and found large differences in predicted runoff, actual evapotranspiration and soil moisture content among models. Consequently, using an ensemble of hydrological models, a larger array of climate projections, different downscaling methods and various bias correction algorithms, is recommended to provide a full range and probability of future hydrologic simulations (Eum et al., 2017; Teutschbein and Seibert, 2012). In addition, the present study was focused on the Manning River catchment, which although deemed to be representative of such catchments, lacks replication at the catchment-scale. Consequently, more catchments will be selected in a following study to represent the large range of climate, physical and flow characteristics throughout Australia, and to provide insights for future water management.

5. Summary and conclusions

This study analysed the hydrologic sensitivity of the Manning River catchment under projected climate change scenarios using the XAJ hydrological model driven by statistically downscaled climate data from 28 GCMs. For the XAJ model calibration and validation periods, the daily NSE were 0.89 and 0.93, and daily R^2 were 0.93 and 0.93, respectively, with monthly NSE ≥ 0.92 and monthly $R^2 \geq 0.94$. Therefore, the XAJ model performed satisfactorily in this catchment (NSE and R^2 were much larger than 0.50). This study explored the impacts of climate change on the water balance of the Manning River catchment for 2040 s and 2080 s. Runoff, actual evapotranspiration and soil moisture content were all largely dominated by rainfall at annual and seasonal time-scales. Maximum temperature was predicted to increase 1.4 °C (1.2–1.5 °C) and 3.2 °C (2.7–3.5 °C) in 2040 s and 2080 s, while minimum temperature was predicted to increase 1.5 °C (1.3–1.7 °C) and 3.5 °C (3.1–4.1 °C) in 2040 s and 2080 s, respectively, as estimated from the median of the 28 GCMs. At an annual time-scale, rainfall, runoff, actual evapotranspiration and soil moisture content were projected to change −0.3% (−5.2–4.2%) and 4.6% (−9.5–10.8%), −2.3% (−10.6–8.9%) and 7.7% (−17.2–22.0%), 0.6% (−3.0–3.7%) and 1.8% (−4.3–8.6%), and −4.4% (−8.8–0.2%) and −5.1% (−15.5 to −1.6%) in 2040 s and 2080 s, respectively. Variations at monthly and seasonal time-scales were also analyzed.

With the trend of increasing values in high rainfall and runoff, and the trend of decreasing values in low rainfall and runoff estimated from the ensemble of the 28 GCMs, a larger degree of inter-seasonal variation in the Manning River catchment are likely to be generated in the future. In addition, reductions in winter runoff and spring and winter soil moisture content in the future are likely to aggravate future water stress for crop growth and productivity (Elmahdi, 2015). These results can potentially contribute to the development of adaptive strategies and future policy options for the sustainable management of water resources in eastern Australia. The research methods used in the Manning River catchment of eastern Australia can be further extended to any other catchments and we expect our study provides helpful reference for climate change impact assessments on water resource management in similar areas.

Declaration of interest

None declared.

Acknowledgements

The first author acknowledges the Chinese Scholarship Council for a scholarship and the NSW Department of Industry for providing office facilities to conduct this work.

We thank the modelling groups, the Program for Climate Model Diagnosis and Intercomparison (PCMDI) and the WCRP's Working Group on Coupled Modelling (WGCM) for their roles in making available the WCRP CMIP5 multi-model dataset. Support of this dataset was provided by the Office of Science, US Department of Energy.

References

Abtew, W., 1996. Evapotranspiration measurements and modeling for three wetland systems in south Florida. Jawra J. Am. Water Resour. Assoc. 32 (3), 465–473.
Ahmed, K.F., Wang, G., Silander, J., Wilson, A.M., Allen, J.M., Horton, R., Anyah, R., 2013. Statistical downscaling and bias correction of climate model outputs for climate change impact assessment in the US northeast. Global Planet. Change 100, 320–332.
Ayele, G.T., Teshale, E.Z., Yu, B., Rutherfurd, I.D., Jeong, J., 2017. Streamflow and sediment yield prediction for watershed prioritization in the Upper Blue Nile River Basin, Ethiopia. Water 9 (10), 782.
Chang, H.J., Jung, I.W., 2010. Spatial and temporal changes in runoff caused by climate change in a complex large river basin in Oregon. J. Hydrol. 388 (3), 186–207.
Chen, H., Xu, C.-Y., Guo, S., 2012. Comparison and evaluation of multiple GCMs, statistical downscaling and hydrological models in the study of climate change impacts on runoff. J. Hydrol. 434, 36–45.
Chiew, F., Whetton, P.H., Mcmahon, T.A., Pittock, A.B., 1995. Simulation of the impacts of climate change on runoff and soil moisture in Australian catchments. J. Hydrol. 167 (1), 121–147.
Chiew, F.H.S., 2006. Estimation of rainfall elasticity of streamflow in Australia. Hydrol. Sci. J. 51 (4), 613–625.
Chiew, F.H.S., Harrold, T.I., Siriwardena, L., Jones, R.N., Srikanthan, R., 2003. Simulation of climate change impact on runoff using rainfall scenarios that consider daily patterns of change from GCMs. In: MODSIM 2003: International Congress on Modelling and Simulation: Proceedings, Modelling and Simulation Society of Australia and New Zealand. ACT, Townsville, pp. 154–159.
Chiew, F.H.S., Mcmahon, T.A., 2002. Modelling the impacts of climate change on Australian streamflow. Hydrol. Process. 16 (6), 1235–1245.
Chiew, F.H.S., et al., 2009. Estimating climate change impact on runoff across southeast Australia: method, results, and implications of the modeling method. Water Resour. Res. 45 (10), 82–90.
Cleverly, J., et al., 2016. The importance of interacting climate modes on Australia's contribution to global carbon cycle extremes. Sci. Rep. 6, 23113.
CSIRO, 2016. State of the climate report 2016, CSIRO and the Bureau of Meteorology, Canberra.
Dar, L.A., 2017. Rainfall-runoff modeling using multiple linear regression technique. Int. J. Res. Appl. Sci. Eng. Technol. 5 (VII), 214–218.
Diaz-Nieto, J., Wilby, R.L., 2005. A comparison of statistical downscaling and climate change factor methods: impacts on low flows in the River Thames, United Kingdom. Clim. Change 69 (2), 245–268.
Duan, Q., Sorooshian, S., Gupta, V.K., 2015. Optimal use of the SCE-UA global optimization method for calibrating watershed models. J. Hydrol. 158 (3–4), 265–284.
Eisner, S., et al., 2017. An ensemble analysis of climate change impacts on streamflow seasonality across 11 large river basins. Clim. Change 141 (3), 1–17.
Elmahdi, A., 2015. Water in Australia 2013 – 14/Bureau of Meteorology, Melbourne.
Eum, H.-I., Yonas, Dibike, Prowse, Terry, 2017. Climate-induced alteration of hydrologic indicators in the Athabasca River Basin, Alberta, Canada. J. Hydrol. 544, 327–342.
Fekete, B.M., Vörösmarty, C.J., Roads, J.O., Willmott, C.J., 2004. Uncertainties in precipitation and their impacts on runoff estimates. J. Clim. 17 (2), 294–304.
Fowler, H.J., Blenkinsop, S., Tebaldi, C., 2007. Linking climate change modelling to impacts studies: recent advances in downscaling techniques for hydrological modelling. Int. J. Climatol. 27 (12), 1547–1578.
Frei, C., et al., 2003. Daily precipitation statistics in regional climate models: evaluation and intercomparison for the European Alps. J. Geophys. Res.: Atmos. 108 (D3), 4124–4143.
Fuss, S., et al., 2015. Betting on negative emissions. Nat. Clim. Change 4 (10), 850–853.
Gan, T.Y., Dlamini, E.M., Biftu, G.F., 1997. Effects of model complexity and structure, data quality, and objective functions on hydrologic modeling. J. Hydrol. 192 (suppl. 1–4), 81–103.
Gardner, L.R., 2009. Assessing the effect of climate change on mean annual runoff. J. Hydrol. 379 (3–4), 351–359.
Gordon, H.B., O'Farrell, S.P., 1997. Transient climate change in the CSIRO coupled model with dynamic sea ice. Mon. Weather Rev. 125 (5), 875–908.
Hao, F., Sun, M., Geng, X., Huang, W., Ouyang, W., 2015. Coupling the Xinanjiang model with geomorphologic instantaneous unit hydrograph for flood forecasting in northeast China. Int. Soil Water Conserv. Res. 3 (1), 66–76.
Hay, L.E., Clark, M.P., 2003. Use of statistically and dynamically downscaled atmospheric model output for hydrologic simulations in three mountainous basins in the western United States. J. Hydrol. 282 (1–4), 56–75.
Hewitson, B., Crane, R., 2006. Consensus between GCM climate change projections with empirical downscaling: precipitation downscaling over South Africa. Int. J. Climatol. 26 (10), 1315–1337.
Hu, C., Guo, S., Xiong, L., Peng, D., 2005. A modified Xinanjiang model and its application in Northern China. Hydrol. Res. 36 (2), 175–192.
Hughes, D.A., 2013. A review of 40 years of hydrological science and practice in southern Africa using the Pitman rainfall-runoff model. J. Hydrol. 501 (20), 111–124.
Hughes, K., Watkins, G., Hughes, K., Kaliska, A., Andersons, L., Boyling, M., 2011. Working With Our Catchment: Manning River Catchment Management Program, MidCoast Water 2011. NSW, Taree.
Huntington, T.G., 2006. Evidence for intensification of the global water cycle: review and synthesis. J. Hydrol. 319 (1–4), 83–95.
IPCC, 2013. Climate change 2013: the physical science basis. contribution of working group i to the fifth assessment report of the intergovernmental panel on climate change. Cambridge University Press, Cambridge, United Kingdom and New York, NY, USA, pp. 710–719.
IPCC, 2014. Climate Change 2014: Synthesis Report. Contribution of Working Groups I, II and III to the Fifth Assessment Report of the Intergovernmental Panel on Climate Change. IPCC, Geneva, Switzerland, pp. 151.
Jayawardena, A.W., Zhou, M.C., 2000. A modified spatial soil moisture storage capacity distribution curve for the Xinanjiang model. J. Hydrol. 227 (1–4), 93–113.
Jiang, T., et al., 2007. Comparison of hydrological impacts of climate change simulated by six hydrological models in the Dongjiang Basin, South China. J. Hydrol. 336 (3–4), 316–333.
Jie, C., Brissette, F.P., Annie, P., Robert, L., 2011. Overall uncertainty study of the hydrological impacts of climate change for a Canadian watershed. Water Resour. Res. 47 (12), 1–16.
Jones, R.N., Chiew, F.H.S., Boughton, W.C., Zhang, L., 2006. Estimating the sensitivity of mean annual runoff to climate change using selected hydrological models. Adv. Water Resour. 29 (10), 1419–1429.
Kachroo, R.K., 1992. River flow forecasting. Part 5. Applications of a conceptual model. J. Hydrol. 133 (1–2), 141–178.
Knutti, R., Furrer, R., Tebaldi, C., Cermak, J., Meehl, G.A., 2010. Challenges in Combining Projections from Multiple Climate Models. J. Clim. 23 (10), 2739–2758.
Le, A.M., Pricope, N.G., 2017. Increasing the accuracy of runoff and streamflow simulation in the Nzoia Basin, Western Kenya, through the Incorporation of satellite-derived CHIRPS Data. Water 9 (2), 114.
Li, H., Zhang, Y., Chiew, F.H.S., Xu, S., 2009. Predicting runoff in ungauged catchments by using Xinanjiang model with MODIS leaf area index. J. Hydrol. 370 (370), 155–162.
Li, H., Zhang, Y., Vaze, J., Wang, B., 2012. Separating effects of vegetation change and climate variability using hydrological modelling and sensitivity-based approaches. J. Hydrol. s 420–421 (7), 403–418.
Lindström, G., Johansson, B., Persson, M., Gardelin, M., Bergström, S., 1997. Development and test of the distributed HBV-96 hydrological model. J. Hydrol. 201 (1–4), 272–288.
Liu, D.L., Zuo, H., 2012. Statistical downscaling of daily climate variables for climate change impact assessment over New South Wales, Australia. Clim. Change 115 (3–4), 629–666.
Liu, L., Xu, H., Wang, Y., Jiang, T., 2017. Impacts of 1.5 and 2 °C global warming on water availability and extreme hydrological events in Yiluo and Beijiang River catchments in China. Clim. Change 10, 1–14.
Manolas, E., 2010. Adapting agriculture to climate change: preparing Australian agriculture, forestry and fisheries for the future. Int. J. Clim. Change Strategies Manage. 2 (3), 362–377.
Mehrotra, R., Sharma, A., 2010. Development and application of a multisite rainfall stochastic downscaling framework for climate change impact assessment. Water Resour. Res. 46 (7), 759–768.
Menzel, L., Bürger, G., 2002. Climate change scenarios and runoff response in the Mulde catchment (Southern Elbe, Germany). J. Hydrol. 267 (1), 53–64.
Minville, M., Brissette, F., Leconte, R., 2008. Uncertainty of the impact of climate change on the hydrology of a nordic watershed. J. Hydrol. 358 (1–2), 70–83.
Nash, J.E., Sutcliffe, J.V., 1970. River flow forecasting through conceptual models part I

— a discussion of principles. J. Hydrol. 10 (3), 282–290.
Nash, L.L., Gleick, P.H., 1991. Sensitivity of streamflow in the Colorado Basin to climatic changes. J. Hydrol. 125 (125), 221–241.
Nelder, J.A., Mead, R., 1965. A simplex method for function minimization. Comput. J. 7 (4), 308–313.
Nielsen, S.A., Hansen, E., 1973. Numerical simulation of the rainfall runoff process on a daily basis. Hydrol. Res. 4 (3), 171–190.
Oki, T., Kanae, S., 2006. Global hydrological cycles and world water resources. Science 313 (5790), 1068–1072.
Pagán, B.R., et al., 2016. Extreme hydrological changes in the southwestern US drive reductions in water supply to Southern California by mid century. Environ. Res. Lett. 11 (9), 094026.
Perrin, C., Michel, C., Andréassian, V., 2003. Improvement of a parsimonious model for streamflow simulation. J. Hydrol. 279 (1), 275–289.
Prudhomme, C., Jakob, D., Svensson, C., 2003. Uncertainty and climate change impact on the flood regime of small UK catchments. J. Hydrol. 277 (1), 1–23.
Reshmidevi, T., Kumar, D.N., Mehrotra, R., Sharma, A., 2018. Estimation of the climate change impact on a catchment water balance using an ensemble of GCMs. J. Hydrol. 556, 1192–1204.
Riahi, K., et al., 2011. RCP 8.5—A scenario of comparatively high greenhouse gas emissions. Clim. Change 109 (1–2), 33.
Richardson, C.W., Wright, D.A., 1984. In: WGEN: a model for generating daily weather variables, ARS-8. U.S. Department of Agriculture, Agricultural Research Service, pp. 83.
Ruelland, D., Ardoin-Bardin, S., Collet, L., Roucou, P., 2012. Simulating future trends in hydrological regime of a large Sudano-Sahelian catchment under climate change. J. Hydrol. s 424–425 (6), 207–216.
Ruprecht, J.E., Peirson, W.L., 2011. In: Stability of the Manning River entrances, Coasts and Ports 2011: Diverse and Developing: Proceedings of the 20th Australasian Coastal and Ocean Engineering Conference and the 13th Australasian Port and Harbour Conference, pp. 641–646.
Sahoo, B., 2005. The Xinanjiang model and its derivatives for modeling soil moisture variability in the land-surface schemes of the climate change models: an overview. Hydrol. Perspect. Sustainable Dev. 518–532.
Sankarasubramanian, A., Vogel, R.M., Limbrunner, J.F., 2001. Climate elasticity of streamflow in the United States. Water Resour. Res. 37 (6), 1771–1781.
Seiller, G., Anctil, F., 2014. Climate change impacts on the hydrologic regime of a Canadian river: comparing uncertainties arising from climate natural variability and lumped hydrological model structures. Hydrol. Earth Syst. Sci. 18 (6), 2033–2047.
Silberstein, R.P., et al., 2012. Climate change and runoff in south-western Australia. J. Hydrol. 475 (12), 441–455.
Sorooshian, S., Duan, Q., Gupta, V.K., 1993. Calibration of rainfall-runoff models: application of global optimization to the Sacramento Soil Moisture Accounting Model. Water Resour. Res. 29 (4), 1185–1194.
Stokes, C., Howden, M., Stokes, C., Howden, M., 2010. Adapting Agriculture to Climate Change: Preparing Australian Agriculture, Forestry and Fisheries for the Future. CSIRO Publishing, Melbourne.
Su, B., Huang, J., Zeng, X., Gao, C., Jiang, T., 2017. Impacts of climate change on streamflow in the upper Yangtze River basin. Clim. Change 141, 1–14.
Tang, J., et al., 2016. Statistical downscaling and dynamical downscaling of regional climate in China: present climate evaluations and future climate projections. J. Geophys. Res. Atmos. 121 (5), 2110–2129.
Tebaldi, C., Knutti, R., 2007. The use of the multi-model ensemble in probabilistic climate projections. Philos. Trans.: Math. Phys. Eng. Sci. 365 (1857), 2053–2075.
Teutschbein, C., Seibert, J., 2012. Bias correction of regional climate model simulations for hydrological climate-change impact studies: review and evaluation of different methods. J. Hydrol. 456, 12–29.
Tian, Y., Xu, Y.P., Zhang, X.J., 2013. Assessment of climate change impacts on river high flows through comparative use of GR4J, HBV and Xinanjiang models. Water Resour. Manage. 27 (8), 2871–2888.
Timbal, B., Fernandez, E., Li, Z., 2009. Generalization of a statistical downscaling model to provide local climate change projections for Australia. Environ. Modell. Software 24 (3), 341–358.
Vaze, J., Teng, J., 2011. Future climate and runoff projections across New South Wales, Australia: results and practical applications. Hydrol. Process. 25 (1), 18–35.
Vu, M., Raghavan, S.V., Liong, S.Y., 2012. SWAT use of gridded observations for simulating runoff–a Vietnam river basin study. Hydrol. Earth Syst. Sci. 16 (8), 2801–2811.
Wang, B., et al., 2017. Spatiotemporal changes in wheat phenology, yield and water use efficiency under the CMIP5 multimodel ensemble projections in eastern Australia. Clim. Res. 72 (2), 83–99.
Wang, G., et al., 2016. Simulating the hydrological responses to climate change of the Xiang River basin, China. Theor. Appl. Climatol. 124 (3–4), 769–779.
Wilby, R.L., Harris, I., 2006. A framework for assessing uncertainties in climate change impacts: low-flow scenarios for the River Thames, UK. Water Resour. Res. 420 (2), 563–575.
Xu, C.Y., Singh, V.P., 2004. Review on regional water resources assessment models under stationary and changing climate. Water Resour. Manage. 18 (6), 591–612.
Yang, Y., et al., 2016. Water use efficiency and crop water balance of rainfed wheat in a semi-arid environment: sensitivity of future changes to projected climate changes and soil type. Theor. Appl. Climatol. 123 (3–4), 565–579.
Yao, C., Zhang, K., Yu, Z., Li, Z., Li, Q., 2014. Improving the flood prediction capability of the Xinanjiang model in ungauged nested catchments by coupling it with the geomorphologic instantaneous unit hydrograph. J. Hydrol. 517 (2), 1035–1048.
Zhang, H., Huang, G.H., 2013. Development of climate change projections for small watersheds using multi-model ensemble simulation and stochastic weather generation. Clim. Dyn. 40 (3–4), 805–821.
Zhang, Y. et al., 2013. Collation of Australian modeller's streamflow dataset for 780 unregulated Australian catchments. Water for a Healthy Country National Research Flagship, 115pp. Catchment Management.
Zhang, Y.Q., Chiew, F.H.S., 2009. Relative merits of different methods for runoff predictions in ungauged catchments. Water Resour. Res. 45 (45), 4542–4548.
Zhao, R., Yilin, Z., Lerun, F., Xinren, L.I.U., Quan, Z., 1980. In: The Xinanjiang model, In Proceedings of the Oxford Symposium. IAHS Publ, pp. 351–356.
Zhao, R.J., 1992. The Xinanjiang model applied in China. J. Hydrol. 135 (1–4), 371–381.